Wall teichoic acids regulate peptidoglycan synthesis by paving cell wall microstructure

Felix Barber[1], Zhe Yuan[1], Zarina Akbary[1], Jacob Biboy[2], Waldemar Vollmer[3], Enrique R. Rojas[1]

1: Center for Genomics and Systems Biology, New York University, New York 10003, United States.

2: Center for Bacterial Cell Biology, Newcastle University, Newcastle upon Tyne NE2 4AX, United Kingdom.

3: Institute for Molecular Bioscience, The University of Queensland, Brisbane, Australia.

Abstract

The Gram-positive cell wall is a rigid polysaccharide-peptide network that bears the cell's turgor pressure and confers cell shape. In rod-shaped bacteria, the Rod complex inserts peptidoglycan polymers into the cell wall circumferentially, generating material anisotropy that promotes anisotropic growth. Wall teichoic acids, an abundant, non-load-bearing component of the Gram-positive cell wall, are also essential for rod-shape for unknown reasons. Here, we report a direct role for wall teichoic acids in anisotropic peptidoglycan synthesis. We show that wall teichoic acids provide a cohesive cell wall substrate that is required for Rod complex activity; conversely, removing wall teichoic acids yields a porous cell wall incapable of sustaining Rod complex activity. Consistent with this, cell elongation and Rod complex motion arrest in cells depleted for wall teichoic acids, but resume following hyperosmotic shocks that contract the cell wall. We further show that cells lacking wall teichoic acids rely instead on the bifunctional peptidoglycan synthesis enzyme PBP1, whose isotropic peptidoglycan synthesis is responsible for the subsequent growth and loss of shape. Taken together, these findings reveal that the microstructure of the Gram-positive cell wall is an essential regulatory factor in its own synthesis.

Summary

The bacterial cell wall is an essential macromolecule that encapsulates the cell and confers cell shape. Here, we reveal that an abundant yet understudied cell wall component in Gram-positive bacteria, wall teichoic acids, facilitates cell wall synthesis in the rod-shaped model organism *Bacillus subtilis* by conferring a physically cohesive substrate for cell wall biosynthetic enzymes. This finding explains the decades-old mystery of why cells that lack wall teichoic acids lose cell shape and grow slowly, while also highlighting an underappreciated factor impacting cell wall homeostasis: the microstructure of the wall itself.

Keywords

Rod complex, bacterial growth, cell shape, peptidoglycan, MreB

Introduction

The bacterial cell wall is a covalently bonded polysaccharide-peptide network that bears the cell's turgor pressure and confers cell shape. This macromolecule consists primarily of peptidoglycan: long glycan polymers that are crosslinked by short peptides[1,2]. Gram-positive bacteria additionally decorate peptidoglycan with negatively charged glycopolymers called wall teichoic acids (hereafter "teichoic acids," distinct from the membrane-bound lipoteichoic acids)[3,4]. Teichoic acids influence diverse cellular functions including antimicrobial resistance[5,6], protein localization within the cell envelope[7], pathogenesis[8], cation homeostasis[9,10] and autolysis[11–14]. In many species they are nonessential[15,16], and have no known structural role in reinforcing the cell wall. However, teichoic acid synthesis is essential for rod-shaped morphogenesis and rapid growth in the Gram-positive model organism, *Bacillus subtilis*, for entirely unknown reasons[15,16].

During cell growth, new peptidoglycan is added to the cell wall by the penicillin binding proteins (PBPs), acting either semi-autonomously or as part of the Rod complex[17,18]. Guided by the actin homolog MreB and its paralogs, Mbl and MreBH[19,20], Rod complexes move circumferentially along the cell

membrane[21–23], polymerizing nascent glycan polymers through transglycosylation reactions catalyzed by RodA[18], and crosslinking their peptides through transpeptidation reactions catalyzed by the class B PBPs PBP2A and PBPH[17,24]. The resulting circumferentially aligned peptidoglycan strands confer the cell wall material anisotropy necessary for rod-shape maintenance[25,26]. Rod complex activity is complemented by the semi-autonomous, bifunctional class A PBPs[17,25], of which the major driver of vegetative growth is PBP1 (encoded by *ponA*). PBP1 is thought to specifically target and fill gaps that arise in the cell wall during normal growth or from cell wall damage[17,27]. Since PBP1 inserts peptidoglycan isotropically, the balance of these distinct peptidoglycan insertion modes sets the cell diameter[25]: the Rod complex decreases cell width while PBP1 increases it.

This model fails to account for the longstanding observation that genetic or pharmacological inhibition of TagO, the enzyme catalyzing the first dedicated step of teichoic acid biosynthesis, causes cells to lose rod shape and confers a severe growth defect[15,16]. One early study observed similar localization patterns for the peptidoglycan and teichoic acid synthetic machinery in *B. subtilis*[28], posing the natural question of whether teichoic acid and peptidoglycan synthesis were coupled[29]. Consistent with this, some studies report that nascent peptidoglycan and teichoic acid synthesis are colocalized both in *B. subtilis*[30] and *Streptococcus pneumoniae*[31]. However, fluorescently tagged teichoic acid-ligases do not exhibit the circumferential motion characteristic of Rod complexes, and Rod complexes still translocate along the cell membrane in amorphous cells depleted for TagO[32,33]. Finally, incomplete teichoic acid synthesis indirectly inhibits peptidoglycan synthesis by sequestering a shared biosynthetic precursor, UndP[33]. However, there is presently no known, direct interaction between teichoic acids and peptidoglycan biosynthesis. Consequently, we have no understanding of why teichoic acid synthesis by TagO is required for cell shape and rapid growth. We address this gap.

Results

Inhibiting wall teichoic acid synthesis reduces growth rate prior to cell shape loss

Prior observations concerning the growth defect of Δ*tagO B. subtilis* cells were limited to bulk culture[16]. To measure the single-cell growth-rate response to acute teichoic acid depletion, we cultured exponentially growing *B. subtilis* cells in microfluidic perfusion chambers and applied low, sublethal doses of the antibiotic tunicamycin to selectively inhibit TagO function[34]. We then monitored the single-cell growth rate using timelapse microscopy. Approximately 9 minutes after tunicamycin treatment, the cellular elongation rate declined from its steady-state level to a lower, basal level that persisted until cell shape loss (Figs. 1A,S1A). Although single-cell tracking became technically challenging upon shape loss, cells continued to grow in this state indefinitely (Video S1).

Tunicamycin inhibits peptidoglycan synthesis and arrests growth at high concentrations of 50 μg/mL[35], while low doses of tunicamycin specifically inhibit TagO[6,36,37]. We performed our experiments with a low tunicamycin concentration (0.5 μg/mL) that inhibits growth to the same extent as deleting *tagO* (Fig. S2A,B) and is not expected to cause off-target effects on peptidoglycan synthesis. However, as a further control for off-target effects, we acutely inhibited transcription of *tagO* and measured the effect on growth rate. To do so, we cultured mutants possessing a single copy of *tagO* under xylose-inducible expression in saturating concentrations of xylose. After rapidly washing out this xylose, we observed a gradual decline in the single-cell growth rate that preceded the loss of cell shape, consistent with our experiments using tunicamycin (Figs. S1B,C).

Inhibiting wall teichoic acid synthesis reduces Rod complex activity

Although it was previously reported that reducing teichoic acid synthesis did not prevent Rod complex activity at steady-state[32], we hypothesized that loss of cell shape could result from a dynamic, transient, effect of teichoic acids on Rod complexes. Since Rod complexes' processive motion along the cell membrane depends on their peptidoglycan synthesis activity[21], Rod complex processive motion is a

common metric for Rod complex-mediated peptidoglycan synthesis[38,39]. We measured Rod complex activity by exposing cells containing an Mbl-sfGFP fusion to 0.5µg/mL tunicamycin and monitoring the response with total internal reflection fluorescence (TIRF) microscopy. Upon tunicamycin treatment, we observed a rapid decline in the percentage of processively moving Rod complexes (Fig. 1B), also evident in kymographs of Mbl motion (Fig. 1B inset). This reduction of Mbl movement was coincident with the initial cell growth decrease during tunicamycin treatment, and remained constant until the loss of cell shape (cf. Fig. 1A). Notably, we observed a slight but reproducible recovery of Rod complex activity following the loss of cell shape (Fig. 1B), consistent with reports of Rod complex activity in *ΔtagO* knockout cells[32]. Visual inspection confirmed the presence of processively motile Mbl-sfGFP puncta after 1h tunicamycin treatment, but with a high level of spatially diffuse Mbl-sfGFP fluorescence relative to normal growth (Fig. S3A and Videos S2-S7).

To control for potential off-target activity of tunicamycin, we monitored Mbl-sfGFP motility in P_{xylA}-*tagO* cells during xylose wash-out. Doing so, we observed a gradual but persistent decline in the percentage of processively moving Mbl filaments (Fig. S3B). Given that tunicamycin rapidly inhibits TagO, while the depletion of *tagO* gene expression relies on growth-mediated dilution of TagO proteins, this gradual decay is consistent with our results in tunicamycin.

Prior studies conflict on whether the spatial density of linearly motile Rod complexes or the average speed of Rod complex processive motion are better metrics for Rod complex activity[38,40]. We tested both, finding similar dynamics upon tunicamycin treatment: a pronounced initial decrease, followed by recovery at later timepoints (Figs. S3C,D). This temporal variability in Rod complex speed was also preserved, though less pronounced, within processively moving Mbl filaments (Fig. S3E). These metrics were also consistent in P_{xylA}-*tagO* cells during xylose depletion (Figs. S3F-H), as well as in wild-type cells containing a distinct, MreB-mNeonGreen fusion (Figs. S3I-L).

We hypothesized that the rapid, coincident reductions of elongation rate and Rod complex movement upon teichoic acid depletion would reduce the rate of Rod complex peptidoglycan synthesis. To test this, we added the fluorescent D-amino acid 'HADA' (7-hydroxycoumarin-3-carboxylic acid-amino-D-alanine) at selected timepoints during tunicamycin treatment. Following HADA wash-out, we measured the average HADA fluorescence intensity within the cell envelope as a readout for peptidoglycan transpeptidation[41,42]. We observed a rapid and reproducible decrease in HADA staining intensity during tunicamycin treatment (Fig. 1C), with aberrant FDAA puncta forming after 30 mins exposure (Fig. 1Ciii). Notably, this decline was preserved in Δ*ponA* cells, in Δ*dacA* cells lacking the principal DD-carboxypeptidase involved in vegetative growth[43], and in P_{xylA}-*TagO* cells during xylose depletion (Fig. S4A). As an orthogonal approach, we purified cell wall isolates and analyzed their composition by high performance liquid chromatography analysis, following prior methods[43] (Fig. S4B). We discovered that the percentage of crosslinked peptide stems for Δ*tagO* cells was reduced relative to wild-type cells (Fig. 1D), consistent with our measurements of FDAA labeling. In sum, these findings demonstrate that Rod complex activity declines during TagO perturbation, either by pharmacological inhibition or dilution, and that this is associated with a PBP1-independent decrease in peptidoglycan crosslinking.

PBP1 is essential without wall teichoic acid synthesis

Since Rod complex activity decreases during teichoic acid depletion, we next tested whether the subsequent growth and loss of cell shape were sustained by PBP1. We grew Δ*ponA* cells (lacking PBP1) in bulk culture with varying concentrations of tunicamycin and measured their optical density at regular intervals with a 96-well plate reader. We also generated and tested cells expressing a mutated variant, $ponA_{S390A}$, that is predicted to lack transpeptidase activity[44], and that accordingly was unlabeled by incubating cells with fluorescently conjugated bocillin (a penicillin analog that covalently binds PBPs *in vivo*[45,46]) (Fig. S5). Both Δ*ponA* and $ponA_{S390A}$ cells showed heightened sensitivity to tunicamycin relative to wild-type cells (Fig. 2A). Furthermore, we observed that while wild-type cells lose shape during

tunicamycin treatment, Δ*ponA* cells do not, and $ponA_{S390A}$ cells displayed only a partial cell shape loss (Fig. 2A inset). To further confirm whether *ponA* was essential in the absence of teichoic acids, we generated Δ*ponA* and $ponA_{S390A}$ mutants in a P_{xylA}-*tagO* background, and assayed cell growth in the presence or absence of xylose using spot-dilution assays (Fig. 2B). We found that both mutants displayed similar growth to wild-type in the presence of xylose, but no growth without, consistent with *ponA* being synthetically lethal with *tagO*. By contrast, cells lacking a functional copy of *pbpD*, the other primary class A PBP involved in vegetative growth, showed a similar growth defect to wild-type cells in the absence of xylose, indicating that this behavior is not generic to class A PBPs (Fig. 2B). Finally, we exposed Δ*ponA* cells to tunicamycin in the presence of propidium iodide: a fluorescent, membrane-impermeable, DNA-binding marker for cell membrane disruption, and monitored cell staining by microscopy. Doing so, we found that Δ*ponA* cells displayed widespread membrane disruption during TagO inhibition (Fig. 2C).

These results demonstrate that PBP1 is responsible for cell growth and shape loss following teichoic acid synthesis inhibition, and support our findings that teichoic acids promote Rod complex activity. To understand when and how this change in the peptidoglycan synthesis modality occurs, we measured the growth dynamics of Δ*ponA* cells treated with tunicamycin. In this condition, we observed a delayed growth rate decline, but no evidence of the subsequent plateau in growth rate that we had observed previously (Fig. 2D cf. Fig. 1A), consistent with PBP1 activity sustaining this plateau in wild-type cells. Notably, in wild-type cells this plateau coincided with the appearance of aberrant FDAA staining (Fig. 1C iii). Next, as a direct metric for PBP1 activity following teichoic acid depletion, we treated live cells with fluorescently conjugated bocillin at several timepoints during tunicamycin treatment and analyzed cell lysates by SDS-PAGE. Doing so revealed a pronounced increase in PBP1 labeling relative to the combined intensity of PBP2A and the cell division PG synthase PBP2B (which could not be distinguished by this assay) (Figs. 2E,F). This is consistent with a relative increase in PBP1 activity or PBP1 availability during TagO inhibition. Finally, to confirm that this increase in PBP1 activity did not drive the temporally associated decline in Rod

complex activity during tunicamycin treatment, we repeated our Mbl tracking in a Δ*ponA* background. We observed a decline in Rod complex motion that was temporally delayed but qualitatively similar to that of wild-type cells (Fig. 2G). Viewed alongside the delayed growth rate decline and the increase in bocillin labeling of PBP1 in wild-type cells, this is consistent with Rod complex-mediated synthesis and growth persisting longer in the absence of an alternative peptidoglycan synthesis modality. We note, however, that the requirement of Δ*ponA* Mbl-sfGFP cells for supplemental magnesium may confound this interpretation. In sum, these findings demonstrate that PBP1 is required for growth and the loss of cell shape during teichoic acid synthesis inhibition, and are consistent with PBP1 activity increasing relative to the combined activity of PBP2A and PBP2B during the same.

Enzymatically digesting wall teichoic acids or peptidoglycan *in vivo* creates a non-growing cell subpopulation

We hypothesized that teichoic acids could facilitate Rod complex activity by stabilizing their interactions with the cell wall. Absent teichoic acids, Rod complexes would then be unable to bridge the resultant pores or 'potholes' on the internal cell wall surface. To begin testing this model, we monitored cell growth while degrading the cell wall in two ways—by perturbing peptidoglycan while leaving teichoic acids intact, and by enzymatically digesting teichoic acids directly. First, we perturbed peptidoglycan by inducing autolysis: cell wall degradation by the cell's native, autolytic enzymes that occurs when cells are incubated in PBS lacking divalent cations[47,48]. Since long periods of autolysis cause cell lysis[47], we used microfluidics to perfuse exponentially growing cells with PBS for only 15 minutes—long enough to arrest growth and increase cell wall permeability (Akbary *et al.*, in submission)—then re-perfused with LB and tracked the growth recovery via microscopy. We observed a growth recovery that plateaued at a slightly decreased rate relative to their steady-state growth (Fig. 3A) (Welch's T-test, P value < 10^{-3}), though with a full recovery in Rod complex activity (Figs. S6A-C). Notably, increasing this PBS incubation time to 30 mins delayed this growth recovery and caused a partial cell growth arrest (Fig. 3B), consistent with our model.

We next sought to determine the relative effect on growth of enzymatically cleaving teichoic acids from the cell wall with a recombinant 'teichoicase', GlpQ. GlpQ is a phosphodiesterase that is secreted in phosphate-starvation conditions to exolytically cleave and recycle teichoic acids from the cell wall[49,50]. Since GlpQ is stereo-specific, it has no activity against the cells' membrane-anchored lipoteichoic acids[50]. We purified recombinant GlpQ using prior methods[49], perfused cells with PBS supplemented with 10µM GlpQ for 15 minutes, and monitored cell growth upon re-perfusion with LB. In stark contrast with the equivalent incubation in PBS alone, we observed that cells treated with native GlpQ split into two distinct subpopulations (Fig. 3C, cf. Fig. 3A): in one, cell growth recovered fully, while in the other, cells remained arrested for the duration of our experiment. Notably, cells that resumed growth did so as rods (Fig. 3Ci) and recovered Rod complex activity (Fig. 3Ciii, Fig. S6D-S6G, Videos S8-S9), while cells that remained arrested consistently showed either diffuse Mbl-sfGFP fluorescence or non-motile fluorescent puncta (Fig. 3Civ, Videos S10-S11). Finally, to determine whether the growth-suppressive effect of GlpQ was titratable, we treated cells with a higher dosage of 40mM GlpQ, finding a full arrest of cell growth upon re-perfusion with LB (Fig. 3D).

We sought to confirm that GlpQ cleaved teichoic acids *in vivo*. To do so, we repeated our 40µM GlpQ treatment in exponentially growing bulk cultures, then labeled teichoic acids by incubating cells with a fluorescently conjugated variant of Concanavalin A—a lectin that binds glycosylation modifications along the teichoic acid polymer[30,51]. Using flow cytometry, we observed that GlpQ-treated cells show decreased Concanavalin A staining relative to PBS-treated cells (Fig.3E) (Welch's T-test, P value < 10^{-3}), consistent with GlpQ enzymatically cleaving teichoic acids from the cell wall as expected. Since GlpQ preferentially cleaves non-glycosylated teichoic acids[49], this fractional reduction in Concanavalin A staining for wild-type cells is likely an underestimate of GlpQ-mediated teichoic acid cleavage. By contrast, Δ*tagO* cells show no such decrease in Concanavalin A staining upon GlpQ incubation, and Δ*tagE* cells lacking the enzyme responsible for teichoic acid glycosylation[52] show negligible labeling. In sum, this data demonstrates that

teichoic acids directly promote Rod complex activity and supports a model in which Rod complexes are inhibited by cell-wall pores resulting from either teichoic acid cleavage or peptidoglycan degradation.

PBP1 is essential for growth recovery following teichoic acid removal

We hypothesized that during TagO inhibition PBP1 not only complements the associated decline in Rod complex activity, but also fills gaps or pores in the peptidoglycan meshwork that would otherwise be occupied by teichoic acids, thereby facilitating the partial recovery of Rod complex motion at long times[32] (Fig. 1B). This hypothesis predicts that Δ*ponA* cells should show a more impaired growth recovery relative to wild-type cells upon direct teichoic acid cleavage using GlpQ, as Rod complexes would be unable to resume their activity without PBP1-mediated pore filling. We tested this prediction, finding that although Δ*ponA* cells treated with denatured GlpQ showed a similar recovery to wild-type following release from autolysis (Fig. 3F, cf. Fig. 3A), Δ*ponA* cells treated with functional GlpQ uniformly failed to recover (Fig. 3G). This finding contrasts severely with the bimodal recovery of wild-type cells at this GlpQ concentration (cf. Fig. 3C). Notably, cell staining with propidium iodide revealed no evidence of systemic lysis following GlpQ treatment (Fig. 3Giv). These findings are consistent with PBP1-mediated insertion filling gaps in peptidoglycan to facilitate Rod complex reactivation following teichoic acid removal.

Wall teichoic acids provide a physically cohesive cell wall substrate for Rod complex activity

If our hypothesis that cell wall pores inhibit Rod complex motion upon teichoic acid removal is correct, then decreasing the size of these pores should increase Rod complex activity, prompting a recovery in cell growth. We tested this prediction by coupling the exit from GlpQ-PBS treatment to a 500mM Sorbitol hyperosmotic shock, physically contracting the cell wall and shrinking any pores resulting from teichoic acid cleavage. To ensure that any cell growth recovery resulted directly from cell wall contraction and not from PBP1 activity, we performed this experiment in Δ*ponA* cells that are otherwise unable to grow

following teichoic acid cleavage. In response to this protocol, we observed a striking, bimodal growth response (Fig. 3H): following the hyperosmotic shock, some cells remained arrested as normal, while others showed the predicted growth recovery. As expected, cells incubated with PBS and subjected to a hyperosmotic shock showed a uniform, prompt growth recovery (Fig. S7).

We sought further confirmation of our hypothesis's assumption that removing teichoic acids generates pores in the cell wall. Notably, prior observations using atomic force microscopy showed differences in internal sidewall architecture of *B. subtilis* sacculi before and after treatment with hydrofluoric acid (HF) to remove teichoic acids[53]: micrographs of HF-treated samples display greater topographical variability within peptidoglycan than those of non-HF-treated samples. Further, the fine structure visible in these micrographs suggests these measurements have sufficient spatial resolution to detect such variations in non-HF-treated sample topography, should they exist. We therefore interpret this difference as supporting the substantial presence of teichoic acids on the internal cell wall surface, whose effect is to smooth out the topography of the underlying peptidoglycan meshwork, consistent with our model.

In sum, these findings support a model in which teichoic acids promote Rod complex activity by filling pores within the peptidoglycan meshwork, that their removal creates pores in the cell wall that impede Rod complex activity, and that PBP1-mediated peptidoglycan synthesis is necessary to restore a sufficiently smooth peptidoglycan substrate for Rod complex activity.

Discussion

Our findings collectively demonstrate that teichoic acids facilitate peptidoglycan synthesis by the Rod complex. Upon TagO inhibition with tunicamycin, we observe a decrease in processively motile Rod complex filament density, and in PBP1-independent transpeptidation, prior to the loss of cell shape. The subsequent shift to PBP1-mediated peptidoglycan synthesis generates an increasingly isotropic cell wall[25] that eventually prompts the loss of cell shape (Fig. 4).

Our experiments with recombinant GlpQ offer a mechanistic explanation for this effect, suggesting that teichoic acids are required for Rod complex activity due to direct yet chemically nonspecific interactions, with their absence impeding Rod complex activity via a 'pothole' model (Fig. 4). Our findings therefore suggest that teichoic acids, despite only being covalently bound to the peptidoglycan meshwork at their base, act in concert with this meshwork to regulate nascent peptidoglycan synthesis: a cohesive cell wall lacking significant gaps promotes further oriented peptidoglycan synthesis, while a porous cell wall arrests Rod complexes in favor of PBP1 synthesis. We further note that this mechanism could be aided by the diverse bridging ionic interactions between teichoic acids and peptidoglycan[54], localizing teichoic acid polymers so as to mask topographical variations within the peptidoglycan meshwork.

We believe our findings on Rod complex activity are compatible with prior observations of motile Rod complexes in Δ*tagO* and TagO-depleted cells[32]. First, we note that the bulk of our observations were made in rod-shaped cells, not spherical cells, allowing us to make quantitative comparisons between wild-type and teichoic acid-depleted cell types without confounding differences in cell geometry. We believe that this methodological difference partly explains why we were able to observe such a stark reduction in Rod complex motion. Additionally, we observed a slight recovery in Rod complex activity upon cell shape loss (Fig. 1B) and visible Rod complex activity after 1h tunicamycin treatment (Videos S6,S7). According to our model, we interpret this recovery as arising from prolonged PBP1 activity generating a state in which the peptidoglycan is sufficiently cohesive to sustain partial Rod complex activity. The fact that cells persist as spheres indefinitely would then indicate that PBP1-mediated synthesis is unable to fully alleviate the porosity resulting from teichoic acids' absence, with Rod complexes consequently serving only a limited role in peptidoglycan synthesis. Notably, this model would explain the longstanding observation that although MreB, Mbl and MreBH are essential in wild-type cells, their deletion causes no significant growth defect in a Δ*tagO* background[55].

We note that although Rod complex activity decreases coincident with the cell growth rate during TagO inhibition, this association does not imply causation. Cell wall hydrolysis ultimately drives cell wall expansion, and must change accordingly. Notably, the key sidewall hydrolase LytE shows a SigI-dependent increase in expression following teichoic acid depletion[56], and recent work has also shown a mechanism of SigI activation consistent with our "pothole" model. Within this mechanism, an intrinsically disordered periplasmic domain on the transmembrane anti-sigma factor RsgI reportedly interacts with peptidoglycan to trigger SigI activation, while a similar intrinsically disordered domain may target PBP1 to holes in the cell-wall[27]. Our model suggests that the same cell wall pores inhibiting Rod complex activity could direct PBP1 synthesis and activate SigI, however, teichoic acids have also been shown to impact hydrolysis by other means[11–14]. Our work to decouple these interactions is ongoing.

The hypothesis that PBP1 synthesis is targeted to peptidoglycan gaps by its intrinsically disordered domain[27] suggests another interpretation of our data: that teichoic acids inhibit PBP1 by preventing its intrinsically disordered domain from interacting with pores in peptidoglycan, and that during teichoic acid depletion, it is increasing PBP1 activity that drives the decrease in Rod complex activity reported here. Notably, the latter part of this hypothesis is incompatible with our finding that Rod complex activity still declines during tunicamycin treatment in cells lacking *ponA* (Fig. 2G). However, it is entirely plausible that the same mechanism by which teichoic acids facilitate Rod complex activity could allow them to inhibit PBP1. This hypothesis is consistent with our observation of increased PBP1 bocillin labeling during tunicamycin treatment, and would position teichoic acids as "master regulators" of peptidoglycan synthesis.

Although we have shown that teichoic acids promote Rod complex motion, it remains unclear whether or how teichoic acid ligation to peptidoglycan is coupled to nascent peptidoglycan synthesis. Our experiments with GlpQ may point to such a coupling. In particular, high levels of teichoic acid cleavage prompt a full growth arrest in cells with both a functional copy of *ponA* and a functional teichoic acid

biosynthesis pathway. This observation may result from PBP1 activity being unable to restart Rod complex activity following sufficiently high levels of teichoic acid cleavage, however it is also consistent with the hypothesis that teichoic acid ligation is coupled to peptidoglycan synthesis. If true, the latter possibility would represent a circular failsafe in Gram-positive cell wall homeostasis, wherein teichoic acids are necessary for oriented peptidoglycan synthesis, while peptidoglycan synthesis is in turn necessary for teichoic acid synthesis. Such a finding would likely indicate greater importance of teichoic acids within the Gram-positive cell wall, well beyond their effects on peptidoglycan synthesis and cell shape as presented here.

Acknowledgements

The authors wish to thank the following people for helpful discussions and insights: Tania Lupoli, Rut Carballido-López, Ethan Garner, Josué Flores-Kim, Sean Wilson and Anna Brogan. We thank Dr Daniela Vollmer for preparation of peptidoglycan. ERR and FB were supported by NSF-CAREER grant 2047404. WV received funding from the UK Biotechnology and Biological Sciences Research Council (BBSRC) (BB/W013630/1).

Author Contributions

FB, ZY and ZA built the strains. FB, ZY, ZA, JB and LPL performed the experiments. FB, ZY, ZA, JB and LPL analyzed the data. FB and ER wrote the manuscript.

Declaration of Interests

The authors declare no competing interests.

Tables

See Table S1 for a list of all strains and primers used in this study.

STAR Methods

Microscopy

All timelapse microscopy was performed with a Nikon Eclipse Ti2 microscope, outfitted with a photometrics PRIME BSI CMOS camera and a Nikon 100X Plan Apo Phase Contrast objective, NA 1.45. All non-TIRF fluorescence imaging used LED illumination. We conducted all imaging using CellASIC ONIX microfluidic plates (Millipore B04A-03), using standard priming and media exchange protocols. We heated all microscope stage components, CellASIC plates, and objectives to 37°C prior to imaging using a microscope incubator outfitted with a heater. We performed our timelapse phase microscopy using 20s timesteps, monitoring medium exchange using the dye AlexaFluor 647 at a final media concentration of 2.5µg/mL, with CY5 illumination adjusted to avoid any confounding effects of photoxicity.

TIRF Microscopy

All TIRF microscopy was performed with the same Nikon Eclipse Ti2 microscope, using a COHERENT 488nm laser and 100X Plan Apo objective, NA 1.45, with 2s timesteps. We adjusted our laser power, exposure time and TIRF alignment to minimize photobleaching, and used a fresh field of view for each new timepoint to avoid any confounding effects of phototoxicity.

Cell culture and transformation

All cell culture was performed in LB media. All *in vivo* imaging and spot-assay experiments were performed with log-phase cultures of OD600≤0.2. Transformations were performed in MC Media + 20mM $MgSO_4$. All cells were congenic with a PY79 strain background. Strains are tabulated in Sheet S1.

Protein purification and application

Protein was purified according to prior methods[49]. We incubated cell cultures of 500mL LB + 100 ug/mL Ampicillin and 35 ug/mL Chloramphenicol at 37°C with shaking until they reached an OD600 of 0.6-0.8.

We shifted these cultures to 16°C, added IPTG (Isopropyl ß-D-1-thiogalactopyranoside) to a final concentration of 0.5mM, and incubated with shaking for 18h. We centrifuged these cultures at 4°C, resuspended in Buffer A (50 mM Tris-HCl + 200 mM NaCl + 1 mM CaCl2 + 1 mM MgCl2, pH 8.0) + +25mM Imidazole and lysed by disruption in an Emulsiflex-C5. After disruption, we incubated the supernatant with a column containing HisPur Ni-NTA Resin (ThermoFisher 88221), ran this column over an Imidazole gradient, and visualized samples via SDS-PAGE with stain-free labeling (BioRad 1610183). We pooled column elutions containing high protein concentrations, performed dialysis at 4°C overnight in Buffer A, concentrated our samples with Amicon Ultra Centrifugal Filters (10KDa molecular weight cutoff), and flash-froze single-use aliquots with liquid Nitrogen for storage at -80°C. We calculated our protein concentration by nanodrop.

The Gram-positive cell wall imposes a substantial diffusion barrier to molecules above 15kDa (Akbary et al., *in submission*). At 30.1kDa, GlpQ exceeds this limit substantially, rendering it necessary to partially degrade the cell wall to allow GlpQ access to its target substrates. As such, we performed all GlpQ incubations in PBS lacking divalent cations, to induce autolysis.

***In vivo* bocillin labeling**

We grew cell cultures to early log-phase, back diluted into prewarmed LB to create multiple identical, log-phase samples, and added tunicamycin (MP Biomedical 0215002805 and Cell Signaling Technology 12819) to each sample at successive time intervals of 10 mins, to a final concentration of 0.5µg/mL. Prior to lysis, we treated all cultures with bocillin-AF647 (Invitrogen, B13233) simultaneously to a final concentration of 1µg/mL, incubated for 2 mins, then pelleted cells for cell lysate extraction. We treated cell pellets with lysis buffer (20mM Tris pH 7.5, 1mM EDTA, 10mM $MgCl_2$, 1mg/mL Lysozyme, 1mM PMSF, 10ug/mL DNAse I, 100ug/mL RNAse A). We added fresh Lysozyme, PMSF, DNAse I and RNAse A to a lysis buffer stock for

each preparation. We then visualized cell lysates via SDS-PAGE (FastCast 10% Acrylamide, Bio-Rad 1610183) using a Cytiva Amersham Typhoon fluorescent imager.

Flow Cytometry

We grew cell cultures to log-phase (OD600=0.1-0.2), then took two samples from a single cell culture, washed 1X in PBS, and incubated in PBS + 40µM GlpQ or PBS + the equivalent volume of Buffer A for 15mins with rocking at 37°C. We then washed cells again 1X in PBS, and resuspended cells in PBS supplemented with 200ug/mL of Concanavalin A-AlexaFluor 647 (Invitrogen, C21421) for 10min at 37°C, with rocking. We washed cells again 1X in PBS, then resuspended samples in PBS for flow cytometry. We performed our flow cytometry measurements with a Cytek Aurora set to 10,000 events per sample, with gains adjusted to capture the full dynamic range of our population measurements. We consistently calibrated the instrument to a low background (<10 events/second), and vigorously vortexed each sample prior to acquisition.

Image Analysis and Tracking

Cell tracking was performed using custom scripts written in ImageJ, MATLAB and Python. Our timelapse image analysis pipeline involved the following steps: image alignment, background removal, and cell tracking based on phase contrast images. Our single timepoint FDAA image analysis pipeline only required background removal and cell segmentation based on phase contrast images, before calculating cellular fluorescence based on background-corrected fluorescence images. All scripts are available for download at: *https://github.com/felixbarber/WTA_Rod_complex_2024*.

MreB filament tracking

We detected and tracked our MreB and Mbl filaments using custom Python scripts written by FB. For filament detection, we used the "blob_log" function within scikit-image's "measure" module, selecting a dynamical threshold throughout each TIRF timecourse to correct for partial photobleaching.

Cell lysis tracking

We tracked cell lysis by perfusing cells with propidium iodide at a final concentration of 2µg/mL, imaging every 5 mins with 100ms RFP at 10% power. Due to a high level of background signal following cell lysis, we annotated cell lysis events semi-automated custom ImageJ macros.

Analysis of peptidoglycan composition

Peptidoglycan was prepared from cell lysates, digested with cellosyl (gift from Hoechst, Germany), and the resulting muropeptides were reduced with sodium borohydride and analyzed by high-performance liquid chromatography as previously described[57].

Data Availability

References

1. Typas, A., Banzhaf, M., Gross, C. A. & Vollmer, W. From the regulation of peptidoglycan synthesis to bacterial growth and morphology. *Nature Reviews Microbiology* **10**, 123–136 (2012).
2. Vollmer, W., Blanot, D. & De Pedro, M. A. Peptidoglycan structure and architecture. *FEMS Microbiol Rev* **32**, 149–167 (2008).
3. Armstrong, J. J., Baddiley, J., Buchanan, J. G. & Carss, B. Nucleotides and the Bacterial Cell Wall. *Nature* **181**, 1692–1693 (1958).
4. Armstrong, J. J. *et al.* Teichoic Acids from Bacterial Walls: Composition of Teichoic Acids from a Number of Bacterial Walls. *Nature* **184**, 247–248 (1959).
5. Brown, S. *et al.* Methicillin resistance in Staphylococcus aureus requires glycosylated wall teichoic acids. *Proc Natl Acad Sci U S A* **109**, 18909–18914 (2012).
6. Campbell, J. *et al.* Synthetic Lethal Compound Combinations Reveal a Fundamental Connection between Wall Teichoic Acid and Peptidoglycan Biosyntheses in Staphylococcus aureus. *ACS Chem. Biol.* **6**, 106–116 (2011).
7. Farha, M. A. *et al.* Inhibition of WTA Synthesis Blocks the Cooperative Action of PBPs and Sensitizes MRSA to beta-Lactams. *ACS Chem. Biol.* **8**, 226–233 (2013).
8. Lu, Y. *et al.* Modulation of MRSA virulence gene expression by the wall teichoic acid enzyme TarO. *Nat Commun* **14**, 1594 (2023).
9. Thomas, K. J. & Rice, C. V. Equilibrium binding behavior of magnesium to wall teichoic acid. *Biochimica et Biophysica Acta (BBA) - Biomembranes* **1848**, 1981–1987 (2015).
10. Wecke, J., Madela, K. & Fischer, W. The absence of D-alanine from lipoteichoic acid and wall teichoic acid alters surface charge, enhances autolysis and increases susceptibility to methicillin in Bacillus subtilis. *Microbiology (Reading)* **143**, 2953–2960 (1997).

11. Bonnet, J. *et al.* Nascent teichoic acids insertion into the cell wall directs the localization and activity of the major pneumococcal autolysin LytA. *The Cell Surface* **2**, 24–37 (2018).
12. Wecke, J., Perego, M. & Fischer, W. d-Alanine Deprivation of Bacillus subtilis Teichoic Acids Is without Effect on Cell Growth and Morphology But Affects the Autolytic Activity. *Microbial Drug Resistance* **2**, 123–129 (1996).
13. Flores-Kim, J., Dobihal, G. S., Fenton, A., Rudner, D. Z. & Bernhardt, T. G. A switch in surface polymer biogenesis triggers growth-phase-dependent and antibiotic-induced bacteriolysis. *eLife* **8**, e44912 (2019).
14. Flores-Kim, J., Dobihal, G. S., Bernhardt, T. G. & Rudner, D. Z. WhyD tailors surface polymers to prevent premature bacteriolysis and direct cell elongation in Streptococcus pneumoniae. *eLife* **11**, e76392 (2022).
15. Boylan, R. J., Mendelson, N. H., Brooks, D. & Young, F. E. Regulation of the Bacterial Cell Wall: Analysis of a Mutant of Bacillus subtilis Defective in Biosynthesis of Teichoic Acid. *Journal of Bacteriology* **110**, 281–290 (1972).
16. D'Elia, M. A., Millar, K. E., Beveridge, T. J. & Brown, E. D. Wall Teichoic Acid Polymers Are Dispensable for Cell Viability in Bacillus subtilis. *Journal of Bacteriology* **188**, 8313–8316 (2006).
17. Cho, H. *et al.* Bacterial cell wall biogenesis is mediated by SEDS and PBP polymerase families functioning semi-autonomously. *Nat Microbiol* **1**, 1–8 (2016).
18. Meeske, A. J. *et al.* SEDS proteins are a widespread family of bacterial cell wall polymerases. *Nature* **537**, 634–638 (2016).
19. Carballido-López, R. *et al.* Actin homolog MreBH governs cell morphogenesis by localization of the cell wall hydrolase LytE. *Dev Cell* **11**, 399–409 (2006).
20. Daniel, R. A. & Errington, J. Control of cell morphogenesis in bacteria: two distinct ways to make a rod-shaped cell. *Cell* **113**, 767–776 (2003).

21. Garner, E. C. *et al.* Coupled, Circumferential Motions of the Cell Wall Synthesis Machinery and MreB Filaments in B. subtilis. *Science* **333**, 222–225 (2011).
22. van Teeffelen, S. *et al.* The bacterial actin MreB rotates, and rotation depends on cell-wall assembly. *Proceedings of the National Academy of Sciences* **108**, 15822–15827 (2011).
23. Domínguez-Escobar, J. *et al.* Processive Movement of MreB-Associated Cell Wall Biosynthetic Complexes in Bacteria. *Science* **333**, 225–228 (2011).
24. Wei, Y., Havasy, T., McPherson, D. C. & Popham, D. L. Rod Shape Determination by the Bacillus subtilis Class B Penicillin-Binding Proteins Encoded by pbpA and pbpH. *Journal of Bacteriology* **185**, 4717–4726 (2003).
25. Dion, M. F. *et al.* Bacillus subtilis cell diameter is determined by the opposing actions of two distinct cell wall synthetic systems. *Nature Microbiology* **4**, 1294–1305 (2019).
26. Garner, E. C. Toward a Mechanistic Understanding of Bacterial Rod Shape Formation and Regulation. *Annual Review of Cell and Developmental Biology* **37**, null (2021).
27. Brunet, Y. R., Habib, C., Brogan, A. P., Artzi, L. & Rudner, D. Z. Intrinsically disordered protein regions are required for cell wall homeostasis in Bacillus subtilis. *Genes Dev* **36**, 970–984 (2022).
28. Formstone, A., Carballido-López, R., Noirot, P., Errington, J. & Scheffers, D.-J. Localization and Interactions of Teichoic Acid Synthetic Enzymes in Bacillus subtilis. *Journal of Bacteriology* **190**, 1812–1821 (2008).
29. Atilano, M. L. *et al.* Teichoic acids are temporal and spatial regulators of peptidoglycan cross-linking in Staphylococcus aureus. *PNAS* **107**, 18991–18996 (2010).
30. Koyano, Y., Okajima, K., Mihara, M. & Yamamoto, H. Visualization of Wall Teichoic Acid Decoration in Bacillus subtilis. *Journal of Bacteriology* **0**, e00066-23 (2023).

31. Bonnet, J. *et al.* One-Pot Two-Step Metabolic Labeling of Teichoic Acids and Direct Labeling of Peptidoglycan Reveals Tight Coordination of Both Polymers Inserted into Pneumococcus Cell Wall. *ACS Chem. Biol.* **13**, 2010–2015 (2018).
32. Hussain, S. *et al.* MreB filaments align along greatest principal membrane curvature to orient cell wall synthesis. *eLife* **7**, e32471 (2018).
33. Schirner, K. *et al.* Lipid-linked cell wall precursors regulate membrane association of bacterial actin MreB. *Nature Chemical Biology* **11**, 38–45 (2015).
34. Bettinger, G. E. & Young, F. E. Tunicamycin, an inhibitor of Bacillus peptidoglycan synthesis: A new site of inhibition. *Biochemical and Biophysical Research Communications* **67**, 16–21 (1975).
35. Tamura, G., Sasaki, T., Matsuhashi, M., Takatsuki, A. & Yamasaki, M. Tunicamycin Inhibits the Formation of Lipid Intermediate in Cell-free Peptidoglycan Synthesis of Bacteria. *Agricultural and Biological Chemistry* **40**, 447–449 (1976).
36. Bracha, R. & Glaser, L. An intermediate in teichoic acid biosynthesis. *Biochemical and Biophysical Research Communications* **72**, 1091–1098 (1976).
37. Hancock, I. C., Wiseman, G. & Baddiley, J. Biosynthesis of the unit that links teichoic acid to the bacterial wall: Inhibition by tunicamycin. *FEBS Letters* **69**, 75–80 (1976).
38. Billaudeau, C. *et al.* Contrasting mechanisms of growth in two model rod-shaped bacteria. *Nature Communications* **8**, 15370 (2017).
39. Sun, Y., Hürlimann, S. & Garner, E. Growth rate is modulated by monitoring cell wall precursors in Bacillus subtilis. *Nat Microbiol* **8**, 469–480 (2023).
40. Sun, Y. & Garner, E. PrkC modulates MreB filament density and cellular growth rate by monitoring cell wall precursors. *bioRxiv* 2020.08.28.272336 (2020) doi:10.1101/2020.08.28.272336.
41. Hsu, Y.-P. *et al.* Fluorogenic d -amino acids enable real-time monitoring of peptidoglycan biosynthesis and high-throughput transpeptidation assays. *Nature Chemistry* **11**, 335–341 (2019).

42. Lupoli, T. J. *et al.* Transpeptidase-Mediated Incorporation of d-Amino Acids into Bacterial Peptidoglycan. *J. Am. Chem. Soc.* **133**, 10748–10751 (2011).

43. Atrih, A., Bacher, G., Allmaier, G., Williamson, M. P. & Foster, S. J. Analysis of peptidoglycan structure from vegetative cells of Bacillus subtilis 168 and role of PBP 5 in peptidoglycan maturation. *J Bacteriol* **181**, 3956–3966 (1999).

44. Sauvage, E. & Terrak, M. Glycosyltransferases and Transpeptidases/Penicillin-Binding Proteins: Valuable Targets for New Antibacterials. *Antibiotics* **5**, 12 (2016).

45. Kocaoglu, O. & Carlson, E. E. Penicillin-Binding Protein Imaging Probes. *Curr Protoc Chem Biol* **5**, 239–250 (2013).

46. Sharifzadeh, S., Dempwolff, F., Kearns, D. B. & Carlson, E. E. Harnessing β-Lactam Antibiotics for Illumination of the Activity of Penicillin-Binding Proteins in Bacillus subtilis. *ACS Chem. Biol.* **15**, 1242–1251 (2020).

47. Jolliffe, L. K., Doyle, R. J. & Streips, U. N. The energized membrane and cellular autolysis in Bacillus subtilis. *Cell* **25**, 753–763 (1981).

48. Dajkovic, A. *et al.* Hydrolysis of peptidoglycan is modulated by amidation of meso-diaminopimelic acid and Mg2+ in Bacillus subtilis. *Molecular Microbiology* **104**, 972–988 (2017).

49. Myers, C. L. *et al.* Identification of Two Phosphate Starvation-induced Wall Teichoic Acid Hydrolases Provides First Insights into the Degradative Pathway of a Key Bacterial Cell Wall Component*. *Journal of Biological Chemistry* **291**, 26066–26082 (2016).

50. Walter, A. *et al.* Phosphoglycerol-type wall and lipoteichoic acids are enantiomeric polymers differentiated by the stereospecific glycerophosphodiesterase GlpQ. *J Biol Chem* **295**, 4024–4034 (2020).

51. Lang, W. K. & Archibald, A. R. Relation between wall teichoic acid content and Concanavalin A binding in Bacillus subtilis 168. *FEMS Microbiology Letters* **20**, 163–166 (1983).

52. Allison, S. E., D'Elia, M. A., Arar, S., Monteiro, M. A. & Brown, E. D. Studies of the genetics, function, and kinetic mechanism of TagE, the wall teichoic acid glycosyltransferase in Bacillus subtilis 168. *J Biol Chem* **286**, 23708–23716 (2011).
53. Pasquina-Lemonche, L. *et al.* The architecture of the Gram-positive bacterial cell wall. *Nature* **582**, 294–297 (2020).
54. Kern, T. *et al.* Dynamics characterization of fully hydrated bacterial cell walls by solid-state NMR: evidence for cooperative binding of metal ions. *J Am Chem Soc* **132**, 10911–10919 (2010).
55. Kawai, Y. *et al.* A widespread family of bacterial cell wall assembly proteins. *The EMBO Journal* **30**, 4931–4941 (2011).
56. Kasahara, J. *et al.* Teichoic Acid Polymers Affect Expression and Localization of dl-Endopeptidase LytE Required for Lateral Cell Wall Hydrolysis in Bacillus subtilis. *Journal of Bacteriology* **198**, 1585–1594 (2016).
57. Sassine, J., Sousa, J., Lalk, M., Daniel, R. A. & Vollmer, W. Cell morphology maintenance in Bacillus subtilis through balanced peptidoglycan synthesis and hydrolysis. *Scientific Reports* **10**, 17910 (2020).
58. Noda, Y., Yoda, K., Takatsuki, A. & Yamasaki, M. TmrB protein, responsible for tunicamycin resistance of Bacillus subtilis, is a novel ATP-binding membrane protein. *Journal of Bacteriology* **174**, 4302–4307 (1992).

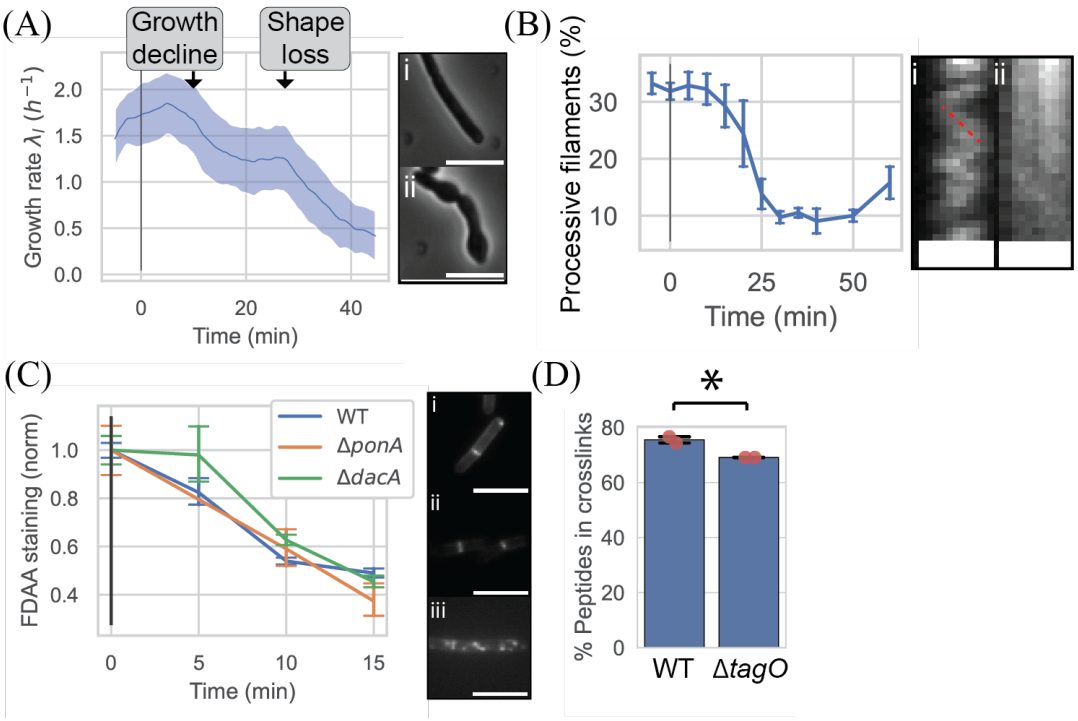

Fig. 1: Inhibiting teichoic acid synthesis decreases Rod complex activity and impedes growth. (A) Cell length growth rate $\lambda_l = \frac{1}{l}\frac{dl}{dt}$ for wild-type cells during 0.5μg/mL tunicamycin treatment. Blue line shows smoothed population median, error bars show standard deviation. Black line shows onset of tunicamycin treatment. Analysis performed over 2,048 discrete cell tracks from 3 biological replicates. Inset: micrographs taken (i) before and (ii) after 45 min tunicamycin treatment. Scale bars 5μm. **(B)** Time course showing the percentage of linearly mobile Mbl filaments during a 0.5μg/mL tunicamycin treatment. Error bars show 95% confidence intervals across biological replicates based on bootstrap analysis. Black line shows onset of tunicamycin treatment. Analysis performed on 62,901 discrete filament tracks from 4 biological replicates. Inset shows representative fluorescent kymographs of Mbl motion across the cell waist in (i) LB and (ii) after 30 min tunicamycin treatment. Red dotted line follows a processive Mbl filament. Scale bars 1μm. **(C)** Normalized mean cell envelope HADA staining for wild-type, Δ*ponA* and Δ*dacA* cells during tunicamycin treatment. Error bars show 95% confidence intervals. Analysis performed over 2,901 segmentations from 3 biological replicates (wild-type), 267 segmentations from two biological replicates (Δ*ponA*), and 2,031 segmentations from 3 biological replicates (Δ*dacA*). Inset shows identically saturated micrographs of wild-type cells at (i) 0 min, (ii) 15 min, and (iii) 30 min of treatment. **(D)** Percentage of peptide stems in peptidoglycan crosslinks as measured on cell walls purified from wild-type and Δ*tagO* cells by HPLC. Two biological replicates per strain. Mean values calculated across biological

replicates. Error bars show 95% confidence intervals. Individual datapoints shown in red. Statistical significance calculated using Student's T-test, $P<0.05$.

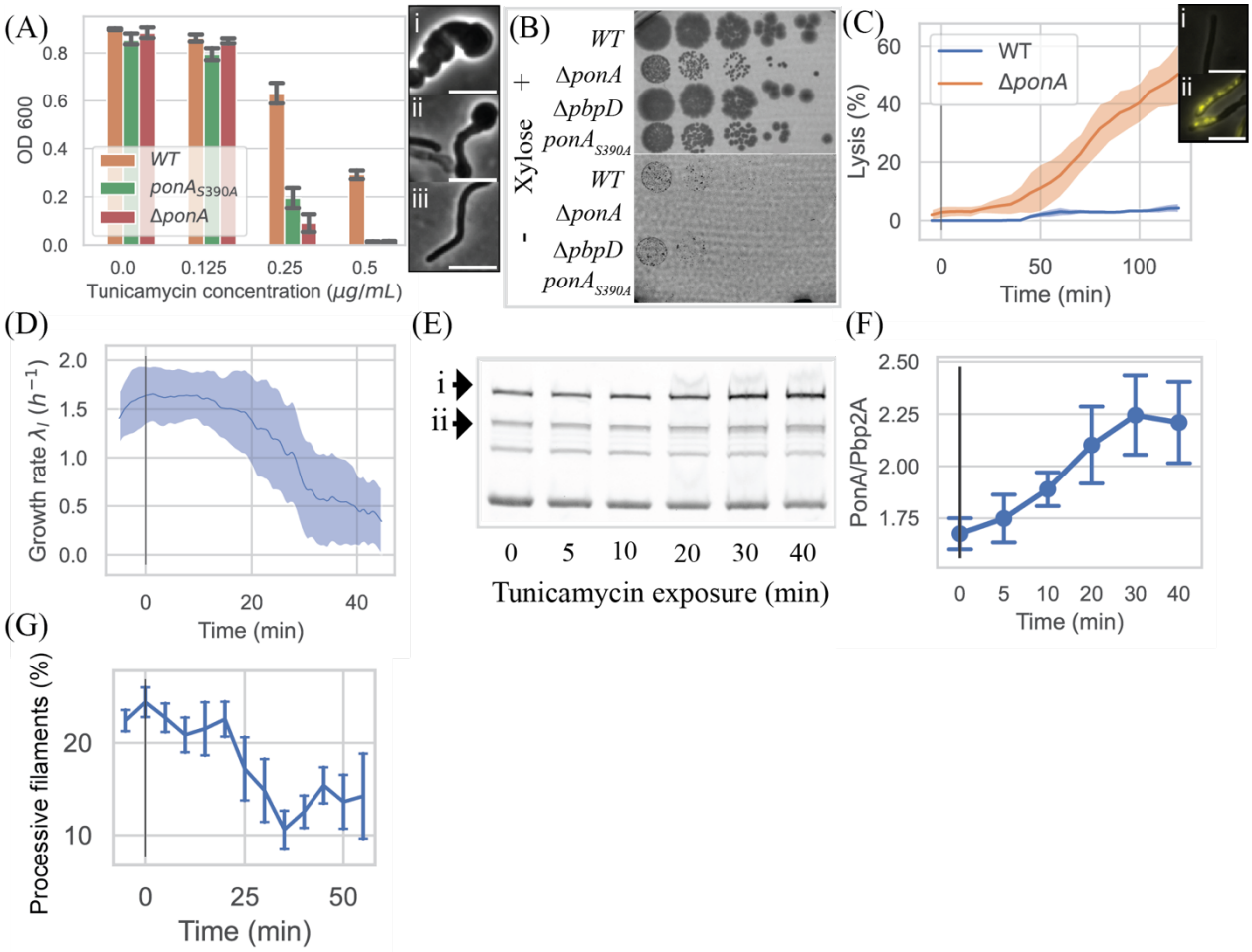

Figure 2: PBP1 is required for growth during teichoic acid synthesis inhibition. (A) Maximum OD for wild-type, Δ*ponA* and $ponA_{S390A}$ (expressing PBP1 with an inactive transpeptidase domain) in varying doses of tunicamycin, grown in bulk culture. Data shown from one representative experiment out of three, with four technical replicates per condition. Inset: micrographs showing (i) wild-type, (ii) $ponA_{S390A}$, (iii) Δ*ponA* cells following 90 min treatment with 0.5µg/mL tunicamycin. Scale bar 5µm. **(B)** Spot assays for P_{xylA}-*tagO*, *ponA* mutant strains grown in the presence and absence of *tagO* induction with 30mM xylose. **(C)** Percentage of membrane-disrupted cells following tunicamycin exposure, measured by propidium iodide staining. Solid line shows mean across all fields of view. Error bars show standard deviation of the same. Black line shows onset of tunicamycin treatment. Analysis performed over 1,098 cells from three biological replicates (Δ*ponA*) and 896 cells from one biological replicate (wild-type). Inset: micrographs showing *ΔponA* cells (i) before and (ii) after 2h tunicamycin treatment. 100X Phase overlaid with propidium iodide stain. Scale bar 5μm. **(D)** Cell length growth rate $\lambda_l = \frac{1}{l}\frac{dl}{dt}$ for Δ*ponA* cells during 0.5µg/mL tunicamycin treatment. Blue line shows smoothed population median, error bars show

standard deviation. Analysis performed over 272 discrete cell tracks from 3 biological replicates. Black line shows onset of tunicamycin treatment. **(E)** SDS-PAGE of *B. subtilis* whole cell lysates shows PBP activity levels during tunicamycin treatment. Arrows show (i) PBP1 and (ii) PBP2A/PBP2B bands. Cells treated with fluorescent bocillin prior to cell lysis. One representative sample shown from 4 biological replicates. **(F)** Quantification of three biological replicates of (E), showing the ratio of PBP1 to PBP2A/PBP2B intensity. Error bars show standard error of the mean across replicates. **(G)** Percentage of processively motile Mbl-sfGFP filaments during tunicamycin treatment of *ΔponA* cells. Error bars show 95% confidence intervals across biological replicates based on bootstrap analysis. Black line shows onset of tunicamycin treatment. Analysis performed on 40,793 discrete filament tracks from three biological replicates.

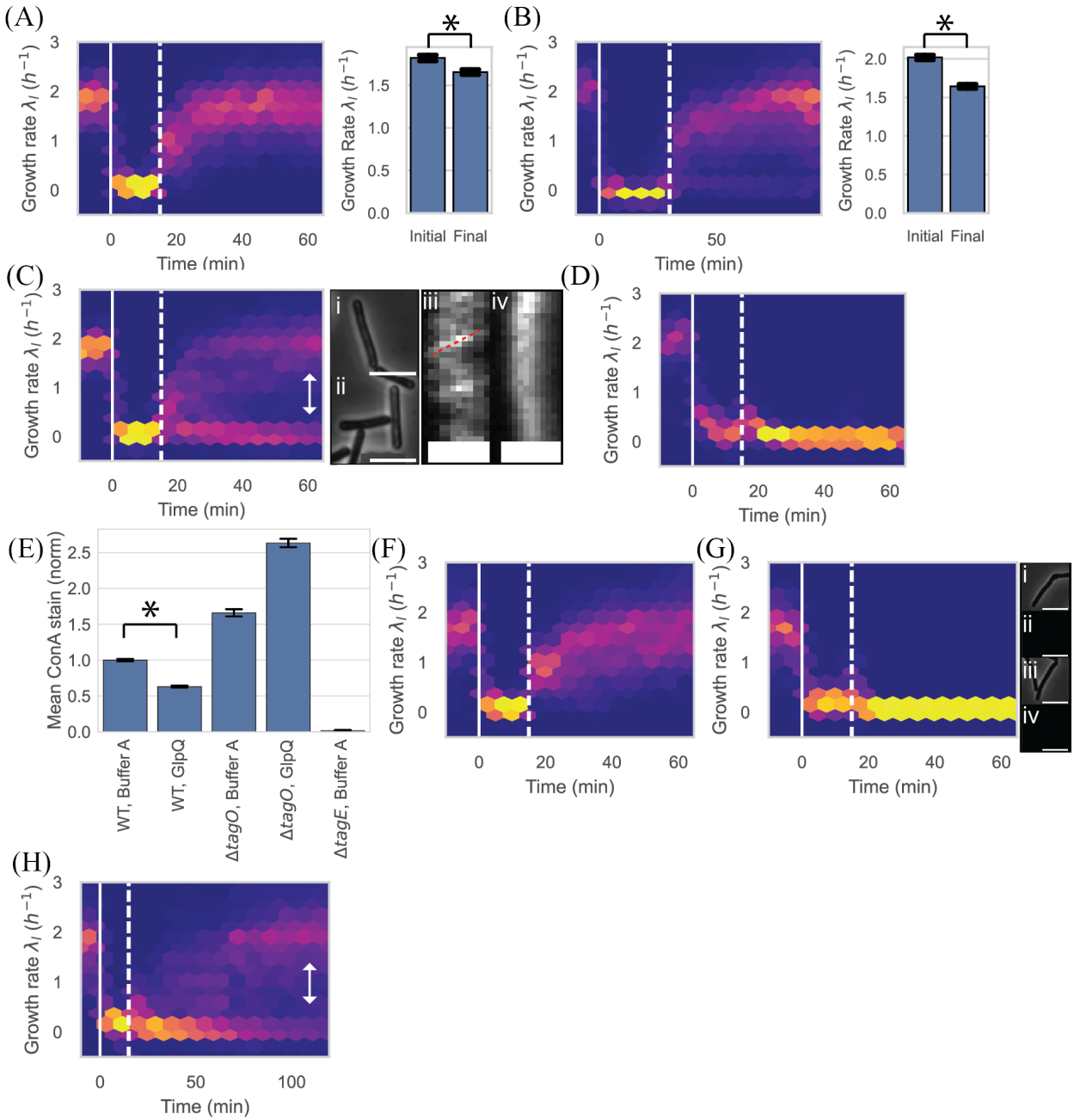

Figure 3: Enzymatically cleaving teichoic acids impedes Rod complex activity and growth in a PBP1 dependent manner. (A-D) Wild-type growth rate $\lambda_l = \frac{1}{l}\frac{dl}{dt}$ during recovery from **(A)** a 15-minute incubation with PBS + denatured GlpQ (3,830 discrete tracks, two independent experiments with denatured GlpQ, one with equivalent volume GlpQ buffer. No differences between conditions observed), **(B)** a 30-minute incubation with PBS + GlpQ buffer (4,394 discrete tracks, three biological replicates), **(C)** a 15-minute incubation with 10µM native GlpQ (3,236 discrete tracks, four biological replicates), or **(D)** a 15-minute incubation with 40µM native GlpQ (1,500 discrete tracks, three biological replicates). To

visualize the bimodal distribution in (C), we plot these growth rate responses as heatmaps, where the intensity shows the number of cells with a given growth rate at a given time, normalized across the total number of cells tracked at each timepoint. Solid line shows onset of PBS perturbation. Dotted line shows exit into LB. Insets in (A) and (B) show the time and population averaged cell growth rate for the initial and final 10 minutes of the timecourses in (A) and (B) respectively. Error bars show 95% confidence intervals by bootstrap analysis. Statistical significance calculated using Welch's T-test, $P<10^{-3}$. Inset in (C) shows (i-ii) cell micrographs of (i) growing and (ii) non-growing cells, and (iii-iv) kymographs of (iii) growing and (iv) non-growing cells, following the exit from GlpQ treatment. Scale bars 5μm in micrographs, 1μm in kymographs. Red dotted line in (iii) follows a processive Mbl filament. **(E)** Mean fluorescence intensity of Concananvalin A-AlexaFluor647 staining, following incubation either with PBS + Buffer A, or with PBS + GlpQ, measured by flow cytometry. Error bars show 95% confidence intervals across 3 biological replicates, 10,000 samples per replicate. Statistical significance measured by Welch's T-test, $P<10^{-3}$. We observed increased Concanavalin A-staining in Δ*tagO* cells relative to wild-type that was amplified during GlpQ treatment, possibly due to the clumping phenotype of this mutant. **(F-I)** Heatmaps showing Δ*ponA* cell length growth rate $\lambda_l = \frac{1}{l}\frac{dl}{dt}$ following a 15-minute incubation with **(F)** PBS (2,142 discrete cell tracks, 3 biological replicates), or **(G)** 10µM GlpQ (1,214 discrete cell tracks, 3 biological replicates). Solid line shows onset of PBS incubation, dotted line shows exit into LB. Inset in (B) shows lack of propidium iodide staining for cells after (i) PBS incubation, (ii) GlpQ incubation. For positive stain, see Fig. 2C ii. **(H)** Heatmap showing Δ*ponA* cell length growth rate $\lambda_l = \frac{1}{l}\frac{dl}{dt}$ following 15-minute incubation with 10µM GlpQ (3,036 discrete cell tracks, 3 biological replicates). Solid line shows onset of PBS incubation, dotted line shows exit into LB + Sorbitol.

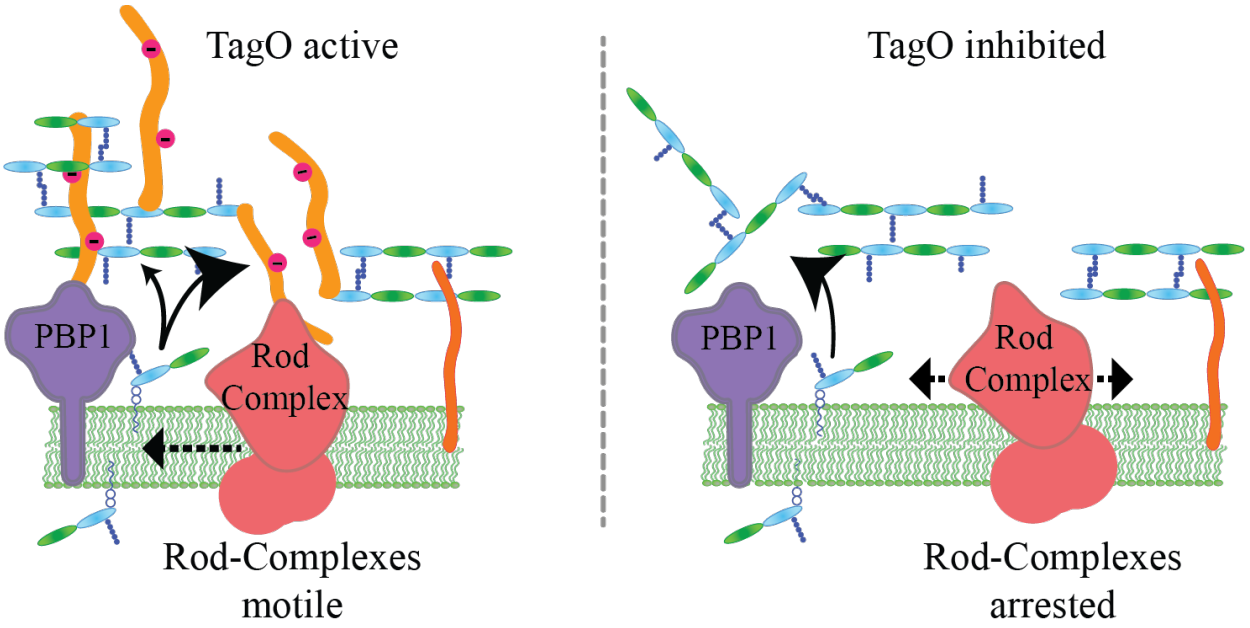

Figure 4: Model. Wall teichoic acids present a cohesive cell wall substrate that facilitates Rod complex mediated peptidoglycan insertion. During teichoic acid cleavage or TagO inhibition, pores in the cell wall destabilize Rod complex activity, causing a redirection of peptidoglycan synthesis to PBP1 that leads to a decline in cell growth and loss of cell shape.